Article

Local Probing ErCrO$_3$

Gonçalo N. P. Oliveira [1,*], Pedro R. Rodrigues [1], João G. Correia [2], João P. E. Araújo [1]
and Armandina M. L. Lopes [1]

1   IFIMUP—Institute of Physics for Advanced Materials, Nanotechnology and Photonics, Departamento de
    Física e Astronomia da Faculdade de Ciências da Universidade do Porto, Rua do Campo Alegre, 687,
    4169-007 Porto, Portugal
2   C2TN—Centro de Ciências e Tecnologias Nucleares, Departamento de Engenharia e Ciências Nucleares,
    Instituto Superior Técnico, Universidade de Lisboa, Bobadela, 2695-066 Boticas, Portugal
*   Correspondence: goliveira@fc.up.pt

Abstract: Local distortions in perovskite-like orthochromites are of extreme importance for the properties they exhibit. Here, we present the results of structural and DC magnetisation measurements combined with local probe studies in polycrystalline ErCrO$_3$. The electric field gradient (EFG) parameters' evolution with temperature shows two clear signals of local environment changes, one at the ferroelectric phase transition (T_{FE}) and the other below 250 K. At the claimed T_{FE}, the EFG changed from a slightly distorted axial symmetric to an EFG with axial symmetry (evidence that the local point-symmetry of the crystal might have changed). At a temperature around 250 K, we observed the development of a magnetic hyperfine field (MHF) and a change in the EFG to an axial slightly distorted one. These observations are rather in line with our magnetisation measurements, as a relatively strong coercive field was observed well above the Cr sub-lattice ordering temperature.

Keywords: perovskite; perturbed angular correlation

1. Introduction

Multifunctional materials, especially with magnetoelectric and multiferroic properties, have attracted great attention in the past decade because of their potential multipurpose applications [1,2]. Rare-earth orthoferrites (RFeO$_3$) and orthochromites (RCrO$_3$), the latter in particular, have been reported to exhibit multiferroic properties due to the local structural inhomogeneity or exchange striction between the rare-earth element and the transition metal ion. In fact, almost a decade ago, Sahu et al. found that rare-earth orthochromites with the formula RCrO$_3$ (R = Ho, Er, Yb, Lu, or Y) exhibit rich and varying physical properties, including octahedral distortions, relaxor-like behaviour, spin-phonon coupling, ferroelectric and multiferroic properties [3–6]. The presence of two magnetic ions and rare-earth magnetic ions' ability to control the orientation of transition metals' magnetic moments originates complex magnetic phases that reflect on their magnetic, optical, and elastic properties. Their complex magnetic structures give rise to interesting magnetic phenomena, such as spin reorientation, a large magnetocaloric effect, and temperature-induced magnetisation reversal.

These materials crystallise in an orthorhombically distorted perovskite-like structure with four distorted perovskite units in the crystallographic cell (space group *Pbnm*)—which forbids ferroeletric ordering, where the strong exchange interaction within the transition metal 3d, Cr^{3+}-Cr^{3+} subsystems is predominantly antiferromagnetic (G type-AFM) and usually orders at higher temperatures (several hundreds of Kelvin) than that of rare-earth 4f, R^{3+}-R^{3+} subsystems—but are also less anisotropic compared to the rare-earth ions. Two other types of anti-ferromagnetic (AFM) exchange couplings can be found in these systems, Cr^{3+}-R^{3+} and R^{3+}-R^{3+}, which account for the numerous fascinating magnetic phenomena present below the Néel temperature. In fact, the coupling plays a decisive role

in determining the different magnetic phases in orthochromites due to spin reorientation transitions, wherein the weak ferromagnetic component becomes parallel to the direction of the applied magnetic field. These several important differences make orthochromites, such as erbium orthochromite $ErCrO_3$, more suitable for the study of phase transitions (magnetic, electric or structural) depending on external stimuli—e.g., temperature, pressure, and applied magnetic fields [7–9]. In reality, only a few papers have reported some of its properties. As far as $ErCrO_3$ is concerned, it presents a magnetic transition in the 113–140 K range and initially was believed to be multiferroic with a claimed ferroelectric (FE) transition in the 472–516 K temperature range, following the condensation of an octahedral tilting mode, which could have a geometric, electronic, and/or magnetic origin [10]. More recently, the works from Meher et al. and Zhu et al. state that a net electric polarisation is observed in $ErCrO_3$ but only below T_N^{Cr}. Furthermore, they show that the paramagnetic nature of the paramagnetic rare-earth site is not necessary to the appearance of ferroelectricity in this system, as was initially believed [11,12].

Clearly, there is a need for further investigations to fully understand the multiferroic and magnetoelectric properties of many chromites. In particular, the origin (or even existence) of the ferroelectric order in these perovskite oxides continues to be shrouded with debate; among such papers is $ErCrO_3$. Given the $ErCrO_3$ complex's nature, where several kinds of order parameters coexist and therefore, are likely to offer new kinds of functionalities, it is worthwhile to study at a local scale the structural, magnetic, and electric properties in order to better grasp the origins of these properties. In this work, we present the results of structural DC magnetisation measurements and perturbed angular correlation for polycrystalline $ErCrO_3$.

2. Materials and Methods

Polycrystalline samples of $ErCrO_3$ were prepared by solid-state reaction of mixed stoichiometric quantities of Er_2O_3 (99.99%, Sigma-Aldrich, Burlington, MA, USA) and Cr_2O_3 (99.9%, Sigma-Aldrich). The mixture was pressed into pellet form, followed by a 15 h heat treatment at 1073 K. Two more grinding and consecutive heating steps were performed at 1573 K (48 h). Phase purity was confirmed by Rietveld refinement of the X-ray powder diffraction data collected with a Panalytical X'Pert Pro diffractometer and analysed with the Fullprof software package [13,14]. The magnetic properties were probed by performing isofield magnetisation curves with a commercial (MPMS Quantum Design) Superconducting Quantum Interference Device (SQUID) magnetometer. See previous work by the authors in reference [14] for further details.

Then, $\gamma - \gamma$ perturbed angular correlation (PAC) spectroscopy [15] was applied to study, at the atomic scale, the structural, electrical, and magnetic properties of this compound. To perform $\gamma - \gamma$ perturbed angular correlation (PAC) spectroscopy [15], individual ~ 0.5 mm^3 samples from the same batch of material were first implanted with ^{111m}Cd ions ($^{111m}Cd \rightarrow {}^{111}Cd$, $t_{1/2} = 48$ min) with a small dose of 10^{11} atoms/cm^2 (dose lower than 1 ppm of the Er/Cr concentration) with 30 keV energy at the ISOLDE-CERN facility (Geneva, Switzerland). Complementary measurements with ^{111}In ions ($^{111}In \rightarrow {}^{111}Cd$, $t_{1/2} = 2.8$ days) introduced into the sample by diffusion process were performed at the Faculty of Sciences of the University of Lisbon. Thermal annealing was performed on all samples, to recover from ^{111m}Cd implantation remaining point defects (for 20 minutes at 973 K) or to promote ^{111}In diffusion (for 48 h at 1273 K), both in an air atmosphere. The crystalline quality of the sample post-implantation annealing process was later rechecked by X-ray diffraction (XRD). A study was performed as a function of temperature (723 K > T > 27 K, ^{111}In), and from (673 K > T > 125 K, ^{111m}Cd), temperature ranges that span over the interesting magnetic phase transitions.

The short lifetime of the parent ^{111m}Cd probe requires that every temperature point is performed after a new implantation-annealing-measurement ~ 4 h cycling. In the case of the ^{111}In probe, the same is not required, allowing the acquisition of multiple temperature data points with a single diffusion. Each temperature measurement took ~ 3 h

of acquisition time using a $6-BaF_2$ detector spectrometer [16] at ISOLDE or in a $4-BaF_2$ detector spectrometer at Lisbon equipped with a dedicated closed-cycle refrigerator or with a special high-temperature furnace. Both ^{111}In and ^{111m}Cd decay to the same PAC probe nuclear excited state ^{111}Cd, with $I = 5/2$ and $Q = 0.664(7)$ [17], by the emission of two consecutive γ rays. The angular correlation between the two γ rays can be perturbed by the EFG and existent magnetic hyperfine fields (B_{hf}). Both the EFG and B_{hf} couple to the nuclear electric quadrupole Q and the magnetic dipole ($\vec{\mu}$) moments of the intermediate nuclear state. The Hamiltonian for such static interactions, in the proper reference frame of the EFG tensor V_{ij}, with $|V_{zz}| > |V_{yy}| > |V_{xx}|$, reads:

$$\mathcal{H} = \frac{\hbar\omega_0}{6}\left[3I_z^2 - I(I+1) + \frac{1}{2}\eta(I_+^2 + I_-^2)\right] + \vec{\mu}\cdot\vec{B}_{hf} \quad , \tag{1}$$

where $\omega_0 = 3eQV_{zz}/[2I(2I-1)\hbar]$ is the fundamental precession frequency, I represents the nuclear spin of the probe intermediate state, $\eta = (V_{xx} - V_{yy})/V_{zz}$ is the EFG asymmetry parameter, and B_{hf} is the magnetic hyperfine field [15,18,19]. Below the antiferromagnetic transition (134 K) of $ErCrO_3$, in the presence of the two fields, we applied combined interaction theory to obtain the B_{hf} and EFG parameters; above T_N, pure static electric quadrupole interactions were considered [20–22].

In the case of a static electric quadrupole interaction, the time-dependent perturbation factor on the observable gamma-ray angular anisotropy of the decay cascade $G_{kk}(t)$, for polycrystalline samples, can be described as a sum of periodic terms, where t is the time spent by the nucleus in the intermediate probing state. In the presence of EFG distributions, the periodic terms are attenuated, here represented by a Lorentzian attenuation function characterised by its relative width δ:

$$G_{kk}(t) = S_{k0} + \sum_n S_{kn}\cos(\omega_n t)e^{-\delta\omega_n t} \quad . \tag{2}$$

The observable ω_n frequencies relate to the energy splitting of the hyperfine levels created when a nuclear state interacts with the external EFG (in the case of ^{111}Cd, the intermediate level is characterised by nuclear spin momentum of $I = 5/2$). The quadrupole interaction splits this level into three ($+/-$ degenerated) sub-levels, which is reason why there is a triplet of frequencies observed in the respective Fourier transform (FT)(ω_1, ω_2, ω_3, where $\omega_3 = \omega_1 + \omega_2$) for each non-vanishing EFG distribution present in the system. The experimental $R(t)$ function can be described, for a static EFG interaction, by $R(t) = \sum A_{kk}G_{kk}(t)$, where A_{kk} are the angular correlation coefficients of the nuclear decay cascade and G_{kk} contains the perturbation terms of the angular correlation. (Further experimental details can be seen in references [18,23]).

3. Results and Discussion

Figure 1a presents the graphical output of the Rietveld refinement performed on the acquired XRD pattern of the $ErCrO_3$ sample after the final heat treatment.

All the diffraction peaks were indexed within the orthorhombic perovskite structure (single phase pattern) belonging to the space group *Pnma*. The obtained values ($a = 5.5091$, $b = 7.5212$, and $c = 5.2275$) are in good agreement with those reported in the literature, evidencing the good quality of the sample [4].

Figure 1b presents the isofield [M(T)] curve for $ErCrO_3$ taken from 5 to 350 K with an applied field of 0.1 kOe (in zero-field cooling—ZFC—and field cooling—FC—modes). The $ErCrO_3$ sample presented an expected behaviour: we observed the Cr^{3+} spins ordering antiferromagnetically below $T_N^{Cr} = 134$ K (Cr^{3+}-Cr^{3+}-exchange interaction dominates), followed by a spin reorientation at 22 K ($\Gamma_4 \rightarrow \Gamma_1$) (the Cr^{3+}-Er^{3+} interaction becomes increasingly important), and finally below, $[6-10]$ K, we observed the ordering of the second magnetic sub-lattice (T_N^{Er}, Er^{3+}), where the Er^{3+}-Er^{3+} interaction enters into consideration. One should point out that the two spin lattices present in the system can be coupled or not. In the case of

a zero-field cooled mode, the Cr^{3+} and Er^{3+} substructures are uncoupled and experience the same external applied field, and thus contribute independently to the total magnetisation. In the FC measuring mode, when the Cr^{3+} sub-lattice moments order at T_N^{Cr}, a local field will be imposed over the Er^{3+} moments. Hence, the Er^{3+} sub-lattice experiences a local field, which is the sum of the internal field due to the Cr^{3+} sub-lattice and the external field. The resulting magnetisation depends on the relative contributions of the sub-lattices and their temperature-dependent magnetic behaviours, hence the difference between the ZFC and FC curves observed in Figure 1b. In the inset, the temperature dependence of the reciprocal magnetic susceptibility data with a linear fit to the paramagnetic region is presented. The Curie-Weiss temperature was found to be $\Theta_P = -39(2)$ K and, also taken from the linear part of the reciprocal susceptibility, an effective paramagnetic moment of 10.4 μ_B was obtained [7,24]. The estimated effective magnetic moment is $\mu = 10.23\ \mu_B$ for $ErCrO_3$ which is close to the theoretical value $\mu_{eff}(ErCrO_3) = 10.35\ \mu_B$ the calculated from the free ion values 9.59 μ_B for Er^{3+} and 3.87 μ_B for Cr^{3+} (spin only values) moments added assuming their total randomness in paramagnetic phase, i.e., $\mu\ (ErCrO_3) = \sqrt{\mu_{Cr^{3+}}^2 + \mu_{Er^{3+}}^2}$.

A weak ferromagnetic moment also arises due to the canting of the Cr^{3+} atoms (for further details on the crystallographic and magnetic characterisation, see reference [25]).
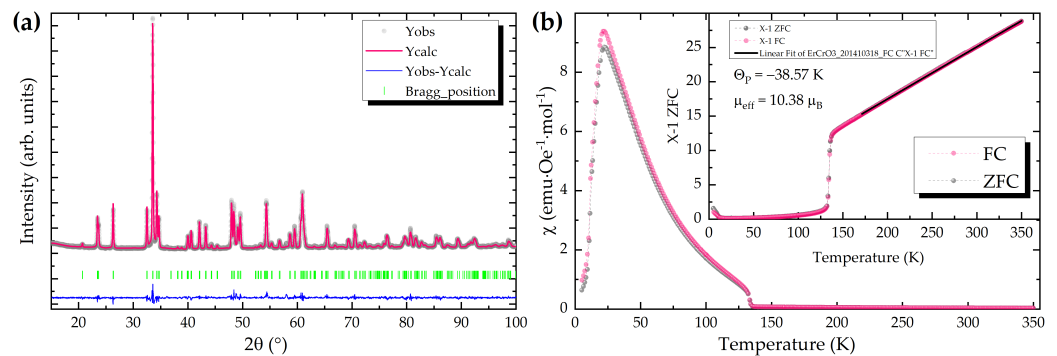

Figure 1. Structural and magnetic characterisation of $ErCrO_3$ sample. (**a**) Room-temperature powder XRD pattern of $ErCrO_3$ sample after the final heat treatment. Experimental pattern (dots), fit curve (pink line), and residual difference (blue line). *Pnma*-phase Bragg reflections (vertical bars). (**b**) $ErCrO_3$ magnetic susceptibility data as a function of temperature measured at 100 Oe, from 5 to 350 K. The inset depicts the reciprocal magnetic susceptibility in the same temperature range. In the reciprocal magnetic susceptibility data, the linear fit to the paramagnetic region is also presented.

Figure 2a depicts the experimental $R(t)$ anisotropy function (left) together with the Fourier transform (right) obtained in the $ErCrO_3$ system using the diffused ^{111}In probe. The global fits to the $R(t)$ functions are shown by the continuous pink lines (thicker ones) in the spectra. Additionally, together with the $R(t)$ spectra are represented lines corresponding to the individual fractions used to perform the fits. Figure 2b shows the same information but for the [111m]Cd PAC probe, but with the representation inverted: left to right and right to left ($R(t)$s and Fts).

The EFG parameters were probed as a function of temperature, T, within the 723 K > T > 27 K interval, which covers the reportedly relevant transition temperatures: ferroelectric transition, the magnetic ordering of the Cr sublattice, and the spin reorientation.

The spectrum obtained at 723 K revealed an EFG characterised by a fundamental frequency of $\omega_0^{Er_1} = 136(1)$ Mrad/s ($V_{zz}^{Er_1} = 77(1)$ V/Å^2) and an asymmetry parameter $\eta^{Er_1} = 0.14(5)$, which are in good agreement with similar systems [26]. A second EFG was used to improve the global fit, characterised by a higher fundamental frequency, $\omega_0^{Er_2} = 171(4)$ Mrad/s ($V_{zz}^{Er_2} = 88(4)$ V/Å^2), and an asymmetry parameter $\eta^{Er_2} = 0.56(9)$.
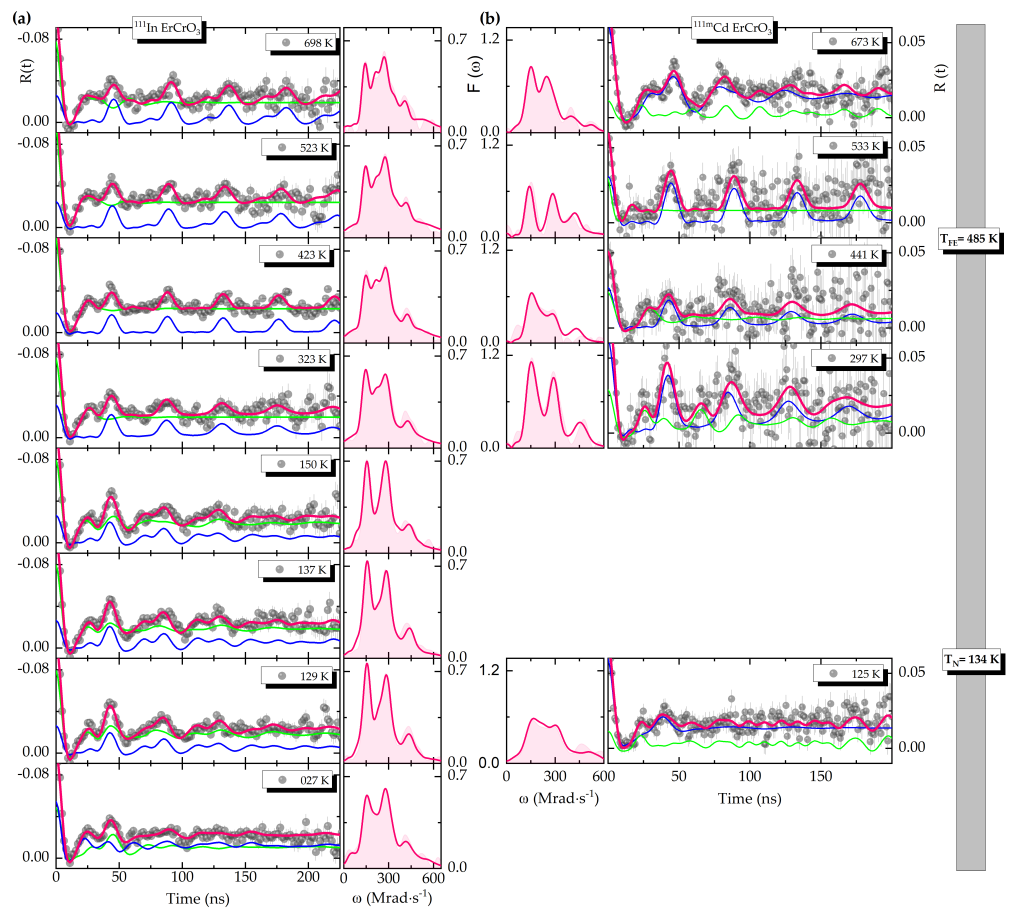
Figure 2. Representative $R(t)$ functions (dots), corresponding fits (thick pink lines), and respective Fourier transform taken at different temperatures for the (**a**) ^{111m}Cd and (**b**) ^{111}In probes in ErCrO$_3$. Thinner blue and green lines represent the individual fractions of the total fit.

In the literature, the works of Junqueira et al., Dogra et al., and Carbonari et al. present similar results to ours. In LaCoO$_3$ and La(Cr, Fe)O$_3$, where the ^{111}In → ^{111}Cd probe was introduced in the samples by a chemical process, two EFG interactions are observed and associated with two non-equivalent crystallographic sites, one associated with the rare-earth site (R) and the other to the Cr and Fe site. Rearick et al. reported that for perovskite systems with heavier R ions, the ^{111m}Cd probe primarily substitutes itself into the rare-earth sites, whereas in systems with lighter R (larger ionic radius), it can be substituted into both the B(Fe, Cr) and the rare-earth sites [27]. Similar findings were obtained in the work of Dogra et al., were only the R site substitution was observed in LaCoO$_3$, whereas for LaCrO$_3$ and (La, Lu, Ho, Eu, Y, Yb)FeO$_3$, both sites were possible [27,28].

Sobolev et al. and Belik et al. also observed similar results—two EFGs, however, in their case. In these works, similar values of V_{zz} and η were observed in systems with different rare-earth atoms [28–31]. In our results we cannot observe any EFG corresponding to probes at the Cr site. We believe that the chemical process used by those authors for introducing the ^{111}In into the samples allows a distribution of the probes by the two lattice sites, whereas by implantation or by diffusion, this does not happen. Furthermore, results of the ab initio calculations show that we should expect a greater V_{zz} value for the rare-earth site and a smaller one for the Cr site ($V_{zz}^R \sim 4V_{zz}^{Cr}$), whereas in the case of the asymmetry parameter, a lower value (low distortion from axial symmetry) should be expected for the R site and a larger value (lack of axial symmetry) for the case of the Cr site. Additionally, we could argue that the presence of the second EFG was indicative of a partial cation inversion between Cr and In sites, as observed in some examples of indium-based 3d-transition metal perovskites [26,32–34], if not for the fact that the study of the dependence of the

EFG parameters and probe distribution as a function of annealing temperature and time showed that the post-implantation/diffusion annealing improves with more time, higher temperatures, and slower cooling (with very slow cooling, the second EFG diminishes drastically, and in some situations even disappears). Thus, we were able to identify that the second EFG observed in this work was due to the post-implantation/diffusion annealing conditions, which is explained in detail in reference [26] and does not have an impact on the results presented here. Thus, it will not be further discussed.

Below T = 473 K the $R(t)$ spectra were fitted with the same EFG^{Er_1} but with a slighter lower asymmetry parameter: $\eta^{Er_2} = 0.04(3)$. When decreasing the temperature even more, below 250 K, in order to be able to perform reasonable fits, we had to consider the scenario where the probes interact now with a magnetic hyperfine field in addition to the EFG. Accordingly, the fits were performed considering a magnetic hyperfine field (combined interactions (EFG+MHF)), even if a weak one. At 250 K, the MHF parameters associated with EFG^{Er_1} are characterised by a Larmor frequency $\omega_L = 2.0$ Mrad/s ($B_{hf} = 0.1$ T) and orientated at an angle of $\beta \approx 60°$ with EFG^{Er_1} principal component $V_{zz}^{Er_1}$. These values increase only marginally as the temperature decreases, and at 125 K we have $\omega_L = 9.4$ Mrad/s ($B_{hf} = 0.6$ T) with the same β. Only well below T_N^{Cr} does the strength of the magnetic interaction become considerable. In this way, at the lowest temperatures measured, 27 and 75 K, the $R(t)$ spectra fit were performed accordingly. EFG^{Er_1} is thus characterised by a fundamental frequency of $\omega_0^{Er_1} = 161(2)$ Mrad/s ($V_{zz}^{Er_1} = 92(2)$ V/Å^2) and an asymmetry parameter of $\eta^{Er_1} = 0.45(8)$. The MHF parameters associated with EFG^{Er_1} are characterised by a Larmor frequency of 44 Mrad/s ($B_{hf} = 3.0$ T) and orientated at $\beta \approx 60°$ with EFG^{Er_1} principal component $V_{zz}^{Er_1}$ (for both temperatures). The data below 250 K, i.e., the presence of an MHF above the magnetic order transition, are rather in line with our magnetisation measurements, as a relatively strong coercive field was observed in this sample well above the Cr^{3+} sub-lattice ordering temperature.

The PAC results using the ^{111m}Cd probe show similar EFGs to those using the ^{111}In parent probe. Above T = 473 K, the $R(t)$ spectra were fitted with the same EFG^{Er_1} but with a higher attenuation parameter. Thus, the parameters obtained were $\omega_0^{Er_1} = 135(5)$ Mrad/s ($V_{zz}^{Er_1} = 77(4)$ V/Å^2) and an asymmetry parameter $\eta^{Er_1} = 0.3(1)$. In the region between T_N^{Cr} and the reported ferroelectric transition (T_{FE}), the observed EFG is characterised by $\omega_0^{Er_1} = 146(5)$ Mrad/s ($V_{zz}^{Er_1} = 84(5)$ V/Å^2) and an asymmetry parameter of $\eta^{Er_1} = 0.01(5)$.

Below T_N^{Cr}, the $R(t)$ spectrum shows strong damping. The final fit solutions were obtained after carefully considering the different tested models and choosing the one that gave the best χ^2 and consistent temperature dependence tendency. In the end, the adopted model was the one considering that the probes interact now with a magnetic hyperfine field in addition to the EFG. Accordingly, the fits were performed considering a magnetic hyperfine field below T_N^{Cr} (combined interactions (EFG+MHF)). Therefore, at 125 K, the spectrum obtained revealed an EFG characterised by a fundamental frequency of $\omega_0^{Er_1} = 157$ Mrad/s ($V_{zz}^{Er_1} = 89$ V/Å^2), an asymmetry parameter $\eta^{Er_1} = 0.25$, and a magnetic component $\omega_L = 13$ Mrad/s ($B_{hf} = 0.8$ T).

The magnetic hyperfine field, measured with ^{111}In or with ^{111m}Cd, is very small. This was not unexpected because we were probing the rare-earth site above its ordering temperature. PAC on similar chromium perovskites (e.g., (Gd, Nd)CrO$_3$) also sustain this observation in the literature [30]. In the cases of GdCrO$_3$ and NdCrO$_3$, both Gd^{3+} and Nd^{3+} ions have incomplete $4f$ shells and in principle should contribute to the hyperfine magnetic field. However, in GdCrO$_3$ and NdCrO$_3$ perovskites measured with ^{181}Ta, the observed B_{hf} values are similar but much smaller than the corresponding value for LaCrO$_3$, where La$_3^+$ has no $4f$-electrons [28,31]. The difference in values observed for these systems may be understood by considering the local magnetic moments of Cr$_3^+$ and rare-earth ions both contributing to hyperfine fields in these compounds.

Let us consider the spin-only value for Cr^{3+} ($3d^3$, $\mu_{eff} = 3.87\ \mu_B$) for the purpose of illustration as the orbital contribution is expected to be largely quenched. In the cases of $RCrO_3$, where Er^{3+} has a zero magnetic moment, only Cr^{3+} moments contribute to the hyperfine field. However, in the case of $RCrO_3$ where R is Nd, Gd, Yb, Er, or Sm, the net effective moment has contributions from the rare-earth moments in addition to the Cr^{3+} moment, and these must be properly taken in to account. The effective moments in these compounds are, however, considerably reduced because Cr^{3+} moments are oriented anti-parallel to those of Er^{3+}, resulting in lower hyperfine fields. It is therefore important to consider the relative importance of Cr^{3+}–R interactions in addition to Cr^{3+}–Cr^{3+} interactions in determining the hyperfine fields in these compounds. The Er^{3+}–Er^{3+} interactions are important only at very low temperatures.

The thermal dependence of the EFGs main parameters (V_{zz} and η) obtained using ^{111}In and ^{111m}Cd probes is depicted in Figure 3a and Figure 3b, respectively.
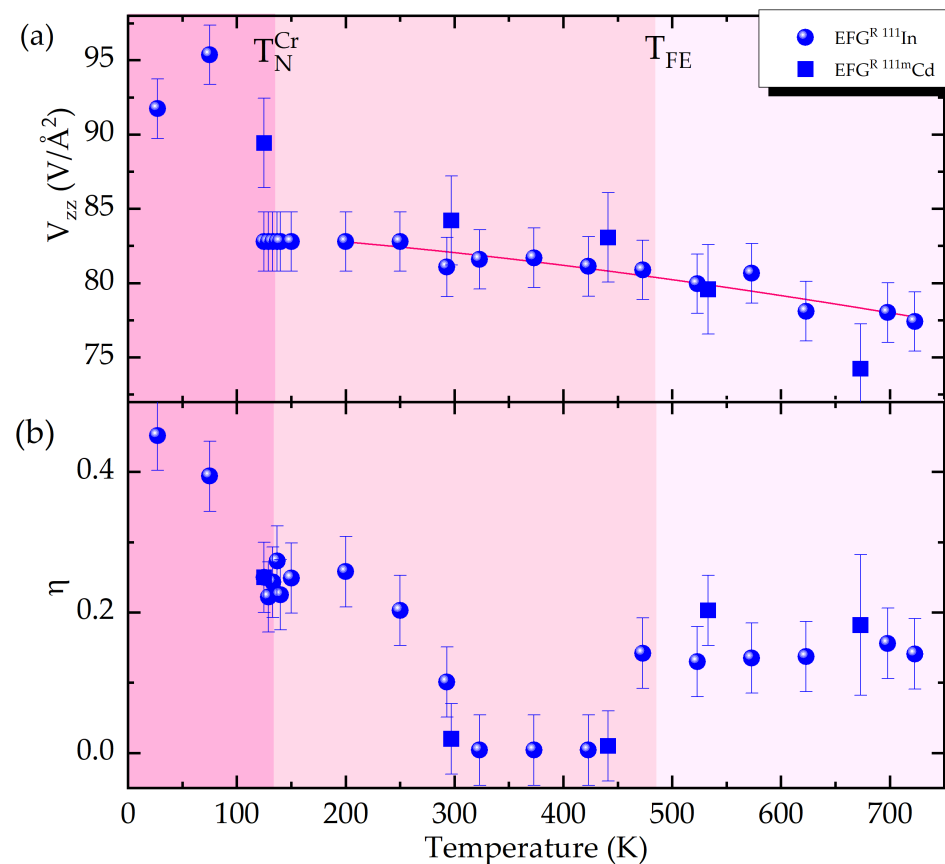

Figure 3. (**a**) Experimental electric field gradient principal component with ^{111}In and ^{111m}Cd probes for the $ErCrO_3$ sample. The continuous line represents a least-squares fit of the function $V_{zz}(T) = V_{zz}(0)(1 + \alpha T^{3/2})$ to the data points. (**b**) Asymmetry parameter.

The EFG attributed to probes substituting Er sites in the lattice measured with ^{111m}Cd and ^{111}In shows a slight monotonic increase in the EFG principal component (V_{zz}) when decreasing the temperature down to T_N^{Cr}. Distinct trends of experimental data on EFG(T) exist; however, the most common is the increase in V_{zz} with decreasing temperature. Although no general description is available, there are several contributions to the temperature dependence of V_{zz}, and their relative magnitude depends strongly on the details of the studied system. Nevertheless, a model proposed by Christiansen et al. [35] shows that in most non-cubic materials, the temperature dependence of the EFG follows the so-called $T^{3/2}$ law: $V_{zz}(T) = V_{zz}(0)\left(1 + \alpha T^{3/2}\right)$, which also fits well in this system. The obtained coefficient for the rare-earth site when fitting V_{zz} is $\alpha^{Er} = 3.6 \times 10^{-6}\ K^{-3/2}$ and is associated with

thermal lattice expansion and atomic vibrations (see solid line in Figure 3a). However, in this temperature span, the asymmetry parameter associated with EFG^{Er_1} seems to present three distinct regimes, the first one above the T_{FE} with $\eta \sim 0.17$; a second between this T_{FE} temperature and 293 K, where an apparent decrease in the value is present ($\eta \sim 0.01$); and a third region where a monotonic increase is present down to the lowest measured temperature. No evident change was observed in the η trend when crossing T_N^{Cr}.

The EFG temperature evolution study on $ErCrO_3$ showed two clear signals of local environment changes, one at the reported T_{FE} and the other just below 250 K. At the claimed ferroelectric phase transition, the EFG changes from a slightly distorted axial symmetry to an EFG with axial symmetry. Naturally, we cannot appoint these changes to a macroscopic crystallographic phase transition or even correlate them with a ferroelectric phase transition, but certainly they provide microscopic evidence that the local point-symmetry of the crystal might have changed. At temperatures around 250 K, we observed the development of an MHF and a change in the EFG to an axial slightly distorted one. These observations are rather in line with our magnetisation measurements, as a relative strong coercive field was observed well above the Cr sub-lattice ordering temperature.

4. Conclusions

The experimental PAC results demonstrate the aptitude of this technique for probing local phenomena. The EFG temperature evolution shows evidence of local environment changes, one at the reported T_{FE} and the other close below 250 K. It is our understanding that our data are compatible with a scenario where local distortions, altering the local symmetry, are sufficient to permit the instalment of a ferroelectric order in this system. We believe that this is a step forward in understanding the exotic behaviour of the $ErCrO_3$ orthochromite with a perovskite structure and its entanglement with lattice distortions.

References

1. Spaldin, N.A.; Cheong, S.W.; Ramesh, R. Multiferroics: Past, present, and future. *Phys. Today* **2010**, *63*, 3–43. [CrossRef]
2. Kimura, T.; Kawamoto, S.; Yamada, I.; Azuma, M.; Takano, M.; Tokura, Y. Magnetocapacitance effect in multiferroic $BiMnO_3$. *Phys. Rev. B* **2003**, *67*, 180401. [CrossRef]
3. Rajeswaran, B.; Khomskii, D.I.; Zvezdin, A.K.; Rao, C.N.R.; Sundaresan, A. Field-induced polar order at the Néel temperature of chromium in rare-earth orthochromites: Interplay of rare-earth and Cr magnetism. *Phys. Rev. B* **2012**, *86*, 214409. [CrossRef]
4. Sahu, J.R.; Serrao, C.R.; Ray, N.; Waghmare, U.V.; Rao, C.N.R. Rare earth chromites: A new family of multiferroics. *J. Mater. Chem.* **2006**, *17*, 4–44. [CrossRef]
5. Serrao, C.; Kundu, A.; Krupanidhi, S.; Waghmare, U.; Rao, C. Biferroic $YCrO_3$. *Phys. Rev. B* **2005**, *72*, 220101. [CrossRef]
6. Bhadram, V.S.; Rajeswaran, B.; Sundaresan, A.; Narayana, C. Spin-phonon coupling in multiferroic $RCrO_3$ (R-Y, Lu, Gd, Eu, Sm): A Raman study. *Europhys. Lett.* **2013**, *101*, 17008. [CrossRef]
7. Tiwari, B.; Surendra, M.K.; Rao, M.S.R. Magnetic phases of erbium orthochromite. *Mater. Res. Express* **2014**, *1*, 036102. [CrossRef]

8. Tiwari, B.; Surendra, M.K.; Rao, M.S.R. HoCrO$_3$ and YCrO3: A comparative study. *J. Phys. Condens. Matter* **2013**, *25*, 21600–216004. [CrossRef]

9. Cooke, A.H.; Martin, D.M.; Wells, M.R. Magnetic interactions in gadolinium orthochromite GdCrO$_3$. *J. Phys. C Solid State Phys.* **2001**, *7*, 3133. [CrossRef]

10. Singh, I.; Nigam, A.K.; Landfester, K.; Muñoz-Espí, R.; Chandra, A. Anomalous magnetic behavior below 10 K in YCrO$_3$ nanoparticles obtained under droplet confinement. *Appl. Phys. Lett.* **2013**, *103*, 182902. [CrossRef]

11. Meher, K.R.S.P.; Wahl, A.; Maignan, A.; Martin, C.; Lebedev, O.I. Observation of electric polarization reversal and magnetodielectric effect in orthochromites: A comparison between LuCrO3 and ErCrO3. *Phys. Rev. B* **2014**, *89*, 144401. [CrossRef]

12. Zhu, Y.; Xia, J.; Wu, S.; Sun, K.; Yang, Y.; Zhao, Y.; Kan, H.W.; Zhang, Y.; Wang, L.; Wang, H.; et al. Crystal growth engineering and origin of the weak ferromagnetism in antiferromagnetic matrix of orthochromates from $t - e$ orbital hybridization. *iScience* **2022**, *25*, 104111. [CrossRef] [PubMed]

13. Rodríguez-Carvajal, J. Recent advances in magnetic structure determination by neutron powder diffraction. *Phys. B Condens. Matter* **1993**, *192*, 5–69. [CrossRef]

14. Oliveira, G.N.P.; Machado, P.; Pires, A.L.; Pereira, A.M.; Araújo, J.P.; Lopes, A.M.L. Magnetocaloric effect and refrigerant capacity in polycrystalline YCrO$_3$. *J. Phys. Chem. Solids* **2016**, *91*, 18–188. [CrossRef]

15. Schatz, G.; Weidinger, A. *Nuclear Condensed Matter Physics: Nuclear Methods and Applications*; Wiley and Sons: Chichester, UK, 1996.

16. Butz, T.; Saibene, S.; Fraenzke, T.; Weber, M. A "TDPAC-Camera". *Nucl. Instruments Methods Phys.* **1989**, *284*, 41–421. [CrossRef]

17. Haas, H.; Röder, J.; Correia, J.G.; Schell, J.; Fenta, A.S.; Vianden, R.; Larsen, E.M.H.; Aggelund, P.A.; Fromsejer, R.; Hemmingsen, L.B.S.; et al. Free Molecule Studies by Perturbed γ-γ Angular Correlation: A New Path to Accurate Nuclear Quadrupole Moments. *Phys. Rev. Lett.* **2021**, *126*, 103001. [CrossRef]

18. Lopes, A.; Araújo, J.P.; Ramasco, J.J.; Amaral, V.S.; Suryanarayanan, R.; Correia, J.G. Percolative transition on ferromagnetic insulator manganites: Uncorrelated to correlated polaron clusters. *Phys. Rev. B* **2006**, *73*. [CrossRef]

19. Barradas, N.P.; Rots, M.; Melo, A.A.; Soares, J.C. Magnetic anisotropy and temperature dependence of the hyperfine fields of ^{111}Cd in single-crystalline cobalt. *Phys. Rev. B* **1993**, *47*, 876–8768. [CrossRef]

20. Ghosh, A.; Dey, K.; Chakraborty, M.; Majumdar, S.; Giri, S. Polar octahedral rotations, cation displacement and ferroelectricity in multiferroic SmCrO3. *EPL* **2014**, *107*, 47012. [CrossRef]

21. Mahana, S.; Manju, U.; Nandi, P.; Welter, E.; Priolkar, K.R.; Topwal, D. Role of local structural distortion in driving ferroelectricity in GdCrO$_3$. *Phys. Rev. B* **2018**, *97*, 224107. [CrossRef]

22. Amrani, M.E.; Zaghrioui, M.; Phuoc, V.T.; Gervais, F.; Massa, N.E. Local symmetry breaking and spin–phonon coupling in SmCrO$_3$ orthochromite. *J. Magn. Magn. Mater.* **2014**, *361*, 1–6. [CrossRef]

23. Lopes, A.M.L.; Araújo, J.P.; Amaral, V.S.; Correia, J.G.; Tomioka, Y.; Tokura, Y. New Phase Transition in the Pr$_{1-x}$Ca$_x$O$_3$ System: Evidence for Electrical Polarization in Charge Ordered Manganites. *Phys. Rev. Lett.* **2008**, *100*, 155702. [CrossRef] [PubMed]

24. Shi, J.; Yin, S.; Seehra, M.S.; Jain, M. Enhancement in magnetocaloric properties of ErCrO$_3$ via A-site Gd substitution. *J. Appl. Phys.* **2018**, *123*, 193901. [CrossRef]

25. Oliveira, G.; Pires, A.; Machado, P.; Pereira, A.; Araújo, J.; Lopes, A. Effect of chemical pressure on the magnetocaloric effect of perovskite-like RCrO$_3$ (R-Yb, Er, Sm and Y). *J. Alloy. Compd.* **2019**, *797*, 26–276. [CrossRef]

26. Oliveira, G.N.P.; Teixeira, R.C.; Moreira, R.P.; Correia, J.G.; Araújo, J.P.; Lopes, A.M.L. Local inhomogeneous state in multiferroic SmCrO$_3$. *Sci. Rep.* **2020**, *10*, 4686. [CrossRef] [PubMed]

27. Rearick, T.M.; Catchen, G.L.; Adams, J.M. Combined magnetic-dipole and electric-quadrupole hyperfine interactions in rare-earth orthoferrite ceramics. *Phys. Rev. B* **1993**, *48*, 22–238. [CrossRef] [PubMed]

28. Dogra, R.; Junqueira, A.C.; Saxena, R.N.; Carbonari, A.W.; Mestnik-Filho, J.; Moralles, M. Hyperfine interaction measurements in LaCrO$_3$ and LaFeO$_3$ perovskites using perturbed angular correlation spectroscopy. *Phys. Rev. B* **2001**, *63*, 224104. [CrossRef]

29. Junqueira, A.C.; Carbonari, A.W.; Saxena, R.N.; Mestnik-Filho, J.; Dogra, R. Temperature dependence of electric field gradient in LaCoO3 perovskite investigated by perturbed angular correlation spectroscopy. *J. Phys. Condens. Matter* **2005**, *17*, 698–6997. [CrossRef]

30. da Silva, R.A.; Saxena, R.N.; Carbonari, A.W.; Cabrera-Pasca, G.A. Investigation of hyperfine interactions in GdCrO$_3$ perovskite oxide using PAC spectroscopy. *Hyperfine Interact.* **2010**, *197*, 5–58. [CrossRef]

31. Carbonari, A.W.; Cavalcante, F.H.M.; Junqueira, A.C.; Leite, D.M.T.; Saxena, R.N.; Mestnik-Filho, J. Investigation of hyperfine interactions in RMO$_3$ (R = La, Nd; M = Cr, Fe) antiferromagnetic perovskite oxides using PAC spectroscopy. *Hyperfine Interact.* **2008**, *178*, 4–49. [CrossRef]

32. Belik, A.A.; Matsushita, Y.; Tanaka, M.; Takayama-Muromachi, E. Crystal Structures and Properties of Perovskites ScCrO$_3$ and InCrO$_3$ with Small Ions at the A Site. *Chem. Mater.* **2012**, *24*, 219–2203. [CrossRef]

33. Sobolev, A.V.; Glazkova, I.S.; Akulenko, A.A.; Sergueev, I.; Chumakov, A.I.; Yi, W.; Belik, A.A.; Presniakov, I.A. ^{61}Ni Nuclear Forward Scattering Study of Magnetic Hyperfine Interactions in Double Perovskites A$_2$NiMnO$_6$ (A = Sc, In, Tl). *J. Phys. Chem. C* **2019**, *123*, 2362–23634. [CrossRef]

34. Sobolev, A.V.; Bokov, A.V.; Yi, W.; Belik, A.A.; Presniakov, I.A.; Glazkova, I.S. Electric Hyperfine Interactions of 57Fe Impurity Atoms in ACrO3 Perovskite-Type Chromites (A = Sc, In, Tl, Bi). *J. Exp. Theor. Phys.* **2019**, *129*, 89–902. [CrossRef]

35. Christiansen, J.; Heubes, P.; Keitel, R.; Klinger, W.; Loeffler, W.; Sandner, W.; Witthuhn, W. Temperature Dependence of the Electric Field Gradient in Noncubic Metals. *Z. Für Phys. B* **1976**, *24*, 17–187. [CrossRef]